

## Analysis of Coupled Lift and Drag forces On Stationary Right Circular Cylinder

Shaikh Jaweed

Department of Mathematics

M. H. Saboo Siddik College of engineering, Byculla, Mumbai, India

e-mail: [javed\\_g@rediffmail.com](mailto:javed_g@rediffmail.com)

Patil Parag

Independent Mathematician, Jalgaon, Maharashtra, India

e-mail: [patilparagv7@gmail.com](mailto:patilparagv7@gmail.com)

Shaikh Feiroz

Shri Jagdishprasad Jhabarmal Tibrewala University, Rajesthan

e-mail: [feiroz.shaikh@gmail.com](mailto:feiroz.shaikh@gmail.com)

**Keywords:** Lift Force, Drag Force, circular cylinder, Higher order spectra, auto-bispectra, auto-trispectra, Nonlinear coupling, Fast Fourier Transform.

A Coupled Lift and Drag analytical model is presented on stationary right circular cylinder in the lock-on regime. Numerical simulations of the flow field are performed on the stationary right circular cylinder to obtain the data for coupled lift and drag coefficients. Spectral analysis is performed to the data to characterize the linear and non-linear coupling between the vortex shedding frequency and its third harmonic. Parameters are obtained on applying Fast Fourier Transform (FFT). From this analysis it is concluded that the van der Pol equation should be used to model the coupled lift and drag coefficients on stationary right circular cylinder in the lock-on regime.

### 1 Introduction

The vortex shedding pattern directly related to drag and lift forces on circular cylinder in their wakes. Reducing vortex induced-vibrations or augmenting the lift component is the area of interest of most of the researchers. To affect the wake pattern and associated forces on the circular cylinder, different forcing conditions have been applied significantly and one such condition is oscillation forcing. Studies by Tokumar and Dimostakis [1], Lu and Sato[2], and Chou[3] on rotationally oscillating cylinder showed a significant drag reduction under specific forcing conditions. Results of Choi et al. [4] showed that the maximum amplitude of the lift coefficient is increased in the lock-on region.

The optimal approach to assess effects of cylinder forcing and the lift and drag forces on the wake structure would be a time-domain numerical simulation of the fluid flow and the structure's motion. On the other hand, and for different purposes such as optimization of the forcing parameters, analytical models have been proposed as a more efficient alternative for determining effects of forces for different conditions of the circular cylinder. One of the first models proposed for vortex-induced vibrations of circular cylinder is the one by Hartlen and Currie [5]. In that model, the lift presented by Rayleigh equation, is linearly coupled to the cylinder's motion. Using a combination of approximate solutions of the Rayleigh and Van der Pol equations and amplitude and phase measurements of higher-order spectral moments, Nayfeh, Owis and Hajj[6] showed that the lift coefficient, on the stationary circular cylinders should be modeled by the self-excited Van der Pol equation. Isam Janajreh and Muhammad Hajj [7] also proved the same result for the lift coefficient, on rotationally oscillating cylinder under the resonance condition. The extension of such models to develop an analytical model for the lift force on in-line oscillating circular cylinder would be very beneficial for modeling vortex-induced vibrations, drag reduction or lift augmentation.

In this model we have presented an analytical model for the prediction of the lift and drag on stationary circular cylinder. Numerical simulations are performed to generate a data base from which parameters for the developed model are determined. Amplitude and phase measurements from higher order spectral parameters are matched with approximate solutions of the model to characterize the nonlinearities in the model and determine these parameters.

### 3 Spectral Analysis

Traditional signal processing techniques used in data analysis are based on second-order statistics, such as the power spectra which are the Fourier transforms of the second-order correlation functions. These quantities yield an estimate of energy content of the different frequency components in a signal or the coherence between equal frequency components in two signals. In many cases, higher-order spectral moments can be used to obtain more information from signals or time series. In nonlinear systems, frequency components interact to pass energy to other components at their sum and/or difference frequency. Because of this interaction, the phases of the interacting components are coupled. This phase coupling can be used for the detection of nonlinear interactions between frequency components in one or more time series. Faced with an unknown system in terms of its nonlinear characteristic, these moments can be applied to identify quadratic and cubic nonlinearities. The bis-spectrum [8, 9, 10], which is the next higher order spectrum to power spectrum, has been established as a tool to quantify the level of phase coupling among three frequency components and thus identify quadratic nonlinearities. To this work our particular interest is the trispectrum [11], which is the next higher order moment to the bis-spectrum, and which is used to detect and characterize cubic nonlinearities expected to be a part of the lift coefficient.

Above induced higher order spectral moments are multi-dimensional Fourier Transforms of higher-order statistical moments. For any real random process  $x(t)$  and its stationary moments up to order  $n$ , one could define the  $n^{\text{th}}$  order moment function as

$$m_n(\tau_1, \tau_2, \tau_3, \dots, \tau_{n-1}) = E\{x(t)x(t + \tau_1) \dots x(t + \tau_{n-1})\} \quad (1)$$

Where  $E\{x\}$  represents ensemble averaging and  $\tau_1, \tau_2, \tau_3, \dots, \tau_{n-1}$  represents time differences.

By Fourier Transforming the second, third and fourth-order moment functions, one obtains, respectively, the auto-power spectrum, auto-bispectrum and auto-trispectrum [11]. Then the hierarchy of higher-order moment spectra is expressed as

$$S_{2x}(f) = \lim_{T \rightarrow \infty} \frac{1}{T} E\{X_T^*(f)X_T(f)\} \quad (2)$$

$$S_{3x}(f_1, f_2) = \lim_{T \rightarrow \infty} \frac{1}{T} E\{X_T^*(f_1)X_T^*(f_2)X_T(f_1 + f_2)\} \quad (3)$$

$$S_{4x}(f_1, f_2, f_3) = \lim_{T \rightarrow \infty} \frac{1}{T} E\{X_T^*(f_1)X_T^*(f_2)X_T^*(f_3)X_T(f_1 + f_2 + f_3)\} \quad (4)$$

Where  $X_T(f)$  is the Fourier Transform of  $x(t)$  define over a time duration  $T$ , and the superscript  $*$  is used to denote complex conjugate. The higher-order spectral moments and their normalized counterparts are capable of identifying nonlinear coupling among frequency components and quantifying their phase relations [8, 9, 10]. In this work, we will stress the use of the auto-trispectrum to determine the phase relation between the vortex shedding component and its third harmonic. This relation will be used in determining the parameters of the proposed analytical model.

#### 4. Numerical Simulation

Direct Numerical simulations of the flow of the unsteady incompressible Navier-Stokes equations for different cases over a stationary circular cylinder were performed. All simulations were performed at  $Re = 100$ . In this simulation the computational domain is extended 15 cylinder diameters upstream, 15 diameters from cross-stream on each side and 40 diameters from downstream. The mesh domain is divided in to multiple blocks in which a quadratic cell type mesh is at the boundaries of the domain and triangular cell type mesh is near the cylinder wall, in order to provide more faces and to enhance the cell communication and computational accuracy. The minimum face area of the cell is  $2.099284e^{-02} m^2$  where as maximum face area is  $6.568327e^{-01} m^2$ . While the minimum Orthogonal Quality and maximum Aspect Ratio are  $6.42237e^{-01}$  and  $6.10345e^{+00}$ . Imposed cylinder oscillations were determined by two parameters, namely, the non-dimensional amplitude,  $Re = \frac{\theta_{max} D v}{2U_{\infty}} = 0.064$ , where  $\theta_{max}$  is the forcing angular velocity, and the forcing frequency  $U_{\infty} = 0.35$ , where  $f$  is the dimensional forcing frequency. Meshing used in this simulation is shown in Fig. 1.

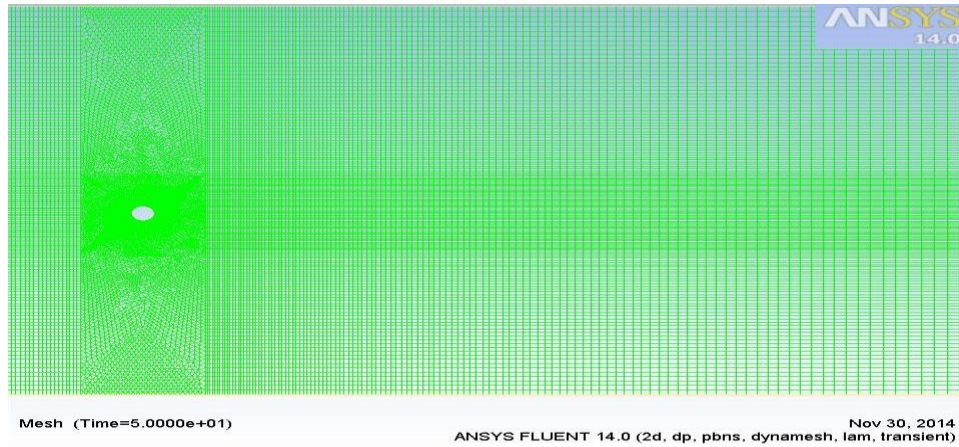


**Fig 1:** Mesh modeling used for the analysis of coupled lift and drag coefficients over the stationary circular cylinder with minimum and maximum face areas of the cell  $2.099284e-02 \text{ m}^2$  and  $6.568327e-01 \text{ m}^2$ . The computational domain extended 15 cylinder diameters upstream, 15 diameters cross-stream on each side and 40 diameters downstream.

Simulations were performed on licensed Ansys fluent software where as the post processing i.e., Fast Fourier Transform (FFT) to obtained spectral parameters were performed on matlab software. Then the validation was done in Microsoft excel software.

#### 4 Analytical Model for the Lift

Analytical models for the prediction of lift coefficient on stationary right circular cylinder modeled by Rayleigh equation and van der Pol oscillator are given by

$$\ddot{C}_L + \omega_s^2 C_L - \mu_r \dot{C}_L + \alpha_r \dot{C}_L^3 = 0 \tag{5}$$

and

$$\ddot{C}_L + \omega_s^2 C_L - \mu_v \dot{C}_L + \alpha_v C_L^2 \dot{C}_L = 0 \tag{6}$$

Where  $\omega_s$  is the shedding frequency,  $(\mu_r, \mu_v)$  and  $(\alpha_r, \alpha_v)$  represents the linear and nonlinear damping coefficients in Rayleigh equation and van der Pol oscillator. The linear and nonlinear damping coefficients are positive so that the linear damping and the nonlinear damping are negative and positive respectively. Because of this stable limit cycles forms, as small and large motions grow and decay.

Analytical approximate solutions, using the method of multiple scales [12, 13], are derived for the equations (5) and (6), and are given below

$$C_L \approx \text{acos}(\omega_s t + \beta) + \frac{\alpha_r \omega_s}{32} a^3 \cos\left(3\omega_s t + 3\beta - \frac{\pi}{2}\right) \tag{7}$$

And

$$C_L \approx a \cos(\omega_s t + \beta) + \frac{\alpha_v}{32\omega_s} a^3 \cos\left(3\omega_s t + 3\beta + \frac{\pi}{2}\right) \quad (8)$$

Where phase  $\beta$  and the amplitude  $a$  for equation (7) are determined by using

$$\dot{a} = \frac{1}{2} \mu_r a - \frac{3\alpha_r \omega_s^2}{8} a^3 \quad (9)$$

$$\dot{\beta} = 0 \quad (10)$$

while for equation (8),  $\beta$  and  $a$  are governed by

$$\dot{a} = \frac{1}{2} \mu_v a - \frac{\alpha_v}{8} a^3 \quad (11)$$

$$\dot{\beta} = 0 \quad (12)$$

When  $a$  and  $\beta$  are constants in equations (7) and (8), i.e., for steady-state oscillations, the solution given in equation (7) and (8) represents a periodic motion which can be written in complex form as

$$C_L(t) \approx \frac{a}{2} \{e^{i(\omega_s t + \beta)} + e^{-i(\omega_s t + \beta)}\} + \frac{\alpha_r \omega_s}{64} a^3 \left\{ e^{i(3\omega_s t + 3\beta - \frac{\pi}{2})} + e^{-i(3\omega_s t + 3\beta - \frac{\pi}{2})} \right\} \quad (13)$$

$$C_L(t) \approx \frac{a}{2} \{e^{i(\omega_s t + \beta)} + e^{-i(\omega_s t + \beta)}\} + \frac{\alpha_v}{64\omega_s} a^3 \left\{ e^{i(3\omega_s t + 3\beta + \frac{\pi}{2})} + e^{-i(3\omega_s t + 3\beta + \frac{\pi}{2})} \right\} \quad (14)$$

The Fourier transform,  $L(\omega)$ , of  $C_L(t)$  presented in (7) and (8) are then given by

$$L(\omega) \approx \frac{a}{2} \{e^{i\beta} \delta(\omega - \omega_s) + e^{-i\beta} \delta(\omega + \omega_s)\} + \frac{\alpha_r \omega_s}{64} a^3 \left\{ e^{i(3\beta - \frac{\pi}{2})} \delta(\omega - 3\omega_s) + e^{-i(3\beta - \frac{\pi}{2})} \delta(\omega + 3\omega_s) \right\} \quad (15)$$

$$L(\omega) \approx \frac{a}{2} \{e^{i\beta} \delta(\omega - \omega_s) + e^{-i\beta} \delta(\omega + \omega_s)\} + \frac{\alpha_v}{64\omega_s} a^3 \left\{ e^{i(3\beta + \frac{\pi}{2})} \delta(\omega - 3\omega_s) + e^{-i(3\beta + \frac{\pi}{2})} \delta(\omega + 3\omega_s) \right\} \quad (16)$$

Examining the expressions for  $L(\omega)$  given in equations (15) and (16), it is noted that the solution thus contains components with frequencies at  $\omega_s$  and  $3\omega_s$ . The amplitudes and phases of these components for equation (15) are given by

$$L(\omega_s) = \frac{a}{2} e^{i\beta} \quad (17)$$

$$L(3\omega_s) = \frac{\alpha_r \omega_s}{64} a^3 e^{i(3\beta - \frac{\pi}{2})} \quad (18)$$

and for equation (16) are given by

$$L(\omega_s) = \frac{a}{2} e^{i\beta} \tag{19}$$

$$L(3\omega_s) = \frac{\alpha_v}{64\omega_s} a^3 e^{i(3\beta+\frac{\pi}{2})} \tag{20}$$

The steady state value of amplitude  $a$  for the Rayleigh and van der Pol equations can be obtained by setting  $\dot{a} = 0$  in equations (9) and (11) i.e.

$$a = \frac{2}{\omega_s} \sqrt{\frac{\mu_r}{3\alpha_r}} \tag{21}$$

$$a = 2 \sqrt{\frac{\mu_v}{\alpha_v}} \tag{22}$$

The auto-trispectrum, which is defined as

$$S_{III}(\omega_k, \omega_l, \omega_m) = \lim_{T \rightarrow \infty} \frac{1}{T} E[L^*(\omega_k)L^*(\omega_l)L^*(\omega_m)L(\omega_k + \omega_l + \omega_m)] \tag{23}$$

is then used to relate the two components,  $\omega_s$  and  $3\omega_s$ . For ( $\omega_k = \omega_l = \omega_m = \omega_s$ ), this relation is given by

$$S_{III}(\omega_s, \omega_s, \omega_s) \approx \frac{a^6 \alpha_r \omega_s}{512} e^{-i\frac{\pi}{2}} \text{ (for Rayleigh equation)} \tag{24}$$

$$S_{III}(\omega_s, \omega_s, \omega_s) \approx \frac{a^6 \alpha_v}{512\omega_s} e^{i\frac{\pi}{2}} \text{ (for van der Pol equation)} \tag{25}$$

From equation (25) it is observed that the magnitude of the auto-trispectrum can be used to determine the coefficient of the cubic nonlinearity  $\alpha_v$ . The phase of the auto-trispectrum  $S_{III}(\omega_s, \omega_s, \omega_s)$ , given by  $\gamma = \phi(3\omega_s) - 3\phi(\omega_s)$ , and equal to  $\frac{\pi}{2}$  or  $-\frac{\pi}{2}$ , should be used to establish the validity of the proposed model.

From equations (7) and (8) it can be clearly observed that there is difference in the phase of the third harmonic in relation to the phase of the vortex shedding frequency. So the correct value of this phase will give the perfect modelling of the lift coefficient. To determine linear and nonlinear damping coefficients in equation (5) from the amplitude and phases of the Fourier components in the time series, the lift coefficient is re-written as

$$C_L \approx a_1 \cos(\omega_s t) + a_3 \cos(3\omega_s t + \gamma) \tag{26}$$

where  $a_1$  and  $a_3$  are the amplitudes of the first and third harmonic, where as  $\gamma$  shows the phase of the third harmonic when phase of the fundamental component is zero. On comparing equations (7), (8) and (26), it can be concluded that lift coefficient  $C_L$  can be modeled either by Rayleigh equation or Van der Pol equation whether  $\gamma = \frac{\pi}{2}$  or  $\gamma = -\frac{\pi}{2}$ .

By comparing equation (26) with equation (8) and applying equation (22), one obtains

$$\alpha_v = \frac{32\omega_s a_3}{a_1^3} \tag{27}$$

$$\mu_v = \frac{1}{4} \alpha_v a_1^2 \tag{28}$$

The mean component that is independent of the lift and a periodic component that is related to the unsteady lift are two components of drag. As the phase relation between the drag component and the lift is near  $3\pi/2$ , hence the periodic component of the drag must be proportional to  $-C_L \dot{C}_L$ .

The drag coefficient can be modeled as

$$d = d_m - \frac{k_1}{a_1^2 \omega_s} C_L \dot{C}_L \tag{29}$$

Where  $d_m$  is mean drag obtained as a mean of time series of the drag and  $k_1$  is the amplitude of the maximum frequency component in the drag. Because the frequency of the major component of the drag is twice the frequency of the major component in the lift, this phase relation is given by  $f(2\omega_s)$  in the drag time series  $-2f(\omega_s)$  in the lift time series. As shown in [6], this phase can be measured as the phase of the cross bispectrum between  $2f$  in the drag and  $f$  in the lift, which is defined as

$$S_{all} = \langle D(2\omega_s) L^*(\omega_s) L(\omega_s) \rangle \tag{30}$$

Where  $D(\omega_s)$  is the Fourier Transform of the drag time series  $d(t)$ .

### 5 Results and Discussion

Vorticity contour in the wake of the stationary right circular cylinder is presented in Fig. 2. In this paper, we have shown validation of the time-varying coupled lift force, which act on a stationary circular cylinder for Reynolds number  $R_e = 100$ . Comparison of vortex shedding pattern presented in Fig. 2 with the pattern, presented in Fig. 3, obtained by Ali H. Nayfeh [6] are nearly similar.

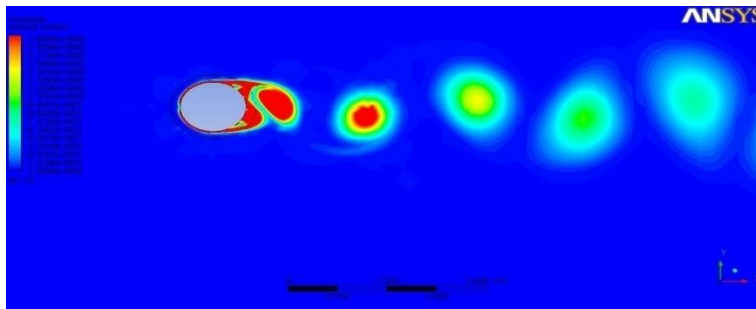


Fig 2: Vorticity contour,  $R_e = 100$ , on stationary right circular cylinder.

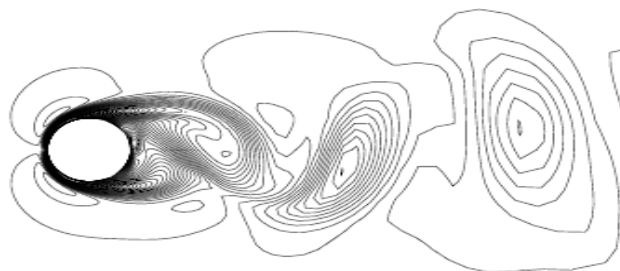
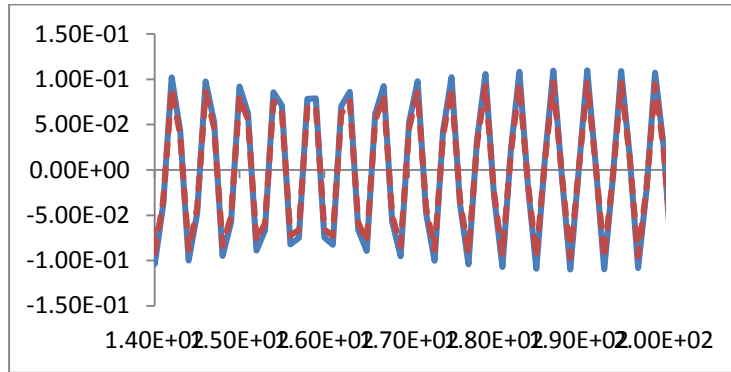
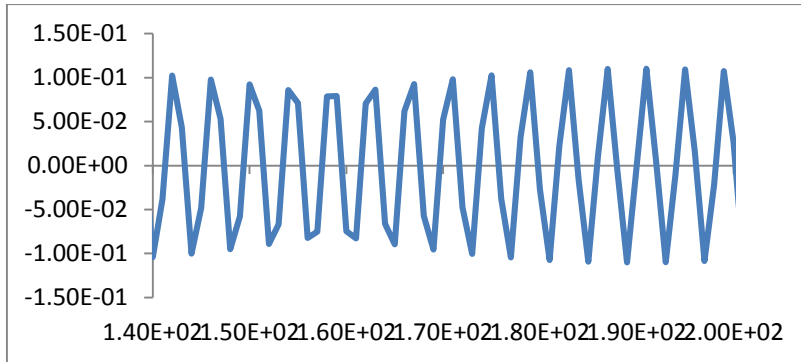


Fig 2: Vorticity contour,  $R_e = 100000$ , on stationary right circular cylinder using RANS by Ali H. Nayfeh [6].



**Fig 3:** Comparison of the analytically modeled (red line) and numerically simulated (blue line) lift time series on stationary circular cylinder. Forcing condition:  $\hat{\theta}_{max}D/2U_{\infty} = 0.064, f_f D/U_{\infty} = 0.35$ .



**Fig 4:** Time histories of the lift coefficient,  $Re = 100$ , on stationary right circular cylinder.

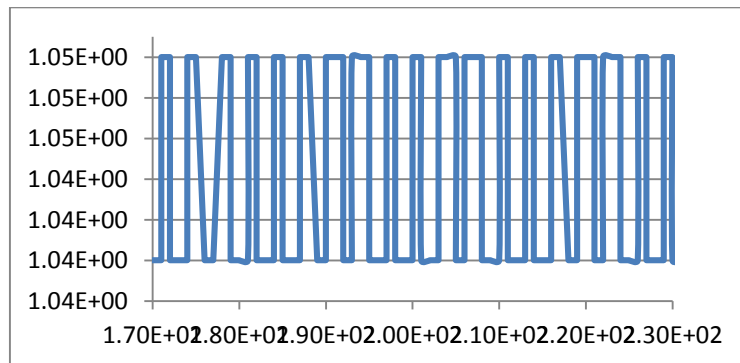


**Fig 5:** Time histories of the drag coefficient,  $Re = 100$ , on stationary right circular cylinder.

Figure 6 show the spectra of the lift coefficient at Reynolds number 100, the spectrum of the lift coefficient shows a major peak at the shedding frequency  $f = 1.546$ . A frequency component at the third harmonic  $3f$  is also present in the spectra of the lift coefficient in Fig 6. It is smaller than the major peak at  $\omega_s$  by three to four orders of magnitude. The presence of peaks corresponding to the shedding frequency and its third harmonic suggests that the lift coefficient on the circular cylinder can be modeled by either the Rayleigh equation or van der Pol equation.

The amplitudes and phases required for the validation of the analytical model presented from van der Pol equation are obtained on applying Fast Fourier Transform (FFT), and the phase and amplitude spectra graphs are shown in Fig 7 and Fig 8. The lift spectral parameters and model parameters obtained on applying FFT are shown in table 1 and table 2.

**Table 1:** Lift spectral parameters in van der Pol equation on stationary circular cylinder.

$y/D$	0.01
$f$ (Hz)	1.546
$a_1$	0.0985
$a_3$	0.0002009
$\phi(\omega_s)$	3.952
$\phi(3\omega_s)$	5.732

**Table 2:** Lift model parameters in van der Pol equation on stationary circular cylinder.

$y/D$	0.01
$f$ (Hz)	1.54633
$\alpha_v$	0.0252
$\mu_v$	10.42
$\gamma$	-6.124

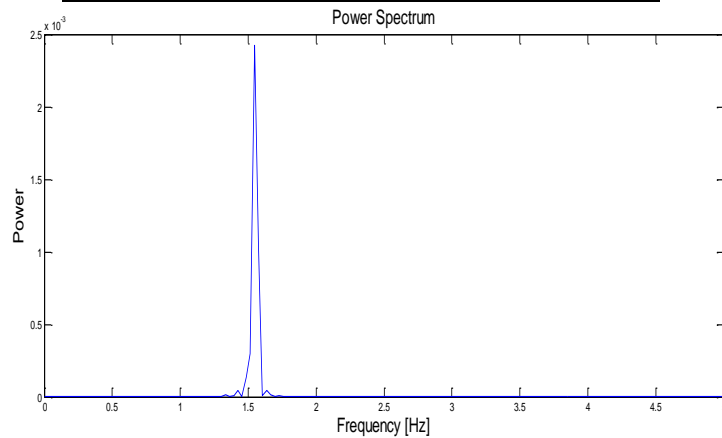


**Fig 6:** Power spectra graph of the numerically simulated lift coefficients from Matlab, on the stationary right circular cylinder:  $\hat{\theta}_{max}D/2U_\infty = 0.064, f_f D/U_\infty = 0.35$

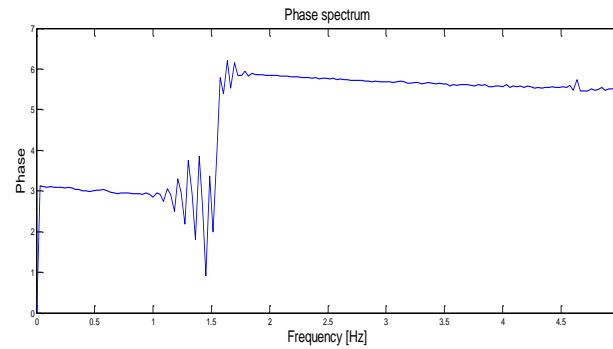


**Fig 7:** Phase spectra graph of the numerically simulated lift coefficients from Matlab, on the stationary right circular cylinder. Forcing condition:  $\dot{\theta}_{\max} D/2U_{\infty} = 0.064$ ,  $f_f D/U_{\infty} = 0.35$

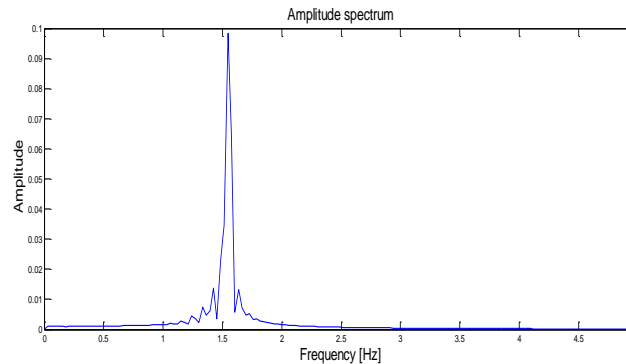


**Fig 8:** Amplitude spectra graph of the numerically simulated lift coefficients from Matlab, on the stationary right circular cylinder. Forcing condition:  $\dot{\theta}_{\max} D/2U_{\infty} = 0.064$ ,  $f_f D/U_{\infty} = 0.35$

## 6 Conclusions

Numerical simulation using Ansys fluent software is performed to validate the analytical model for the lift on stationary right circular cylinder. Fast Fourier Transform (FFT) is performed on Matlab for the validation of the purposed lift model. The perfect matching of the lift time series shows that Rayleigh equation and Van der Pol oscillator would be used to model the lift on a stationary right circular cylinder.

## REFERENCES

- [1] P. T. Tokumaru and P. E. Dimotakis. Rotary oscillation control of a cylinder wake. *J. Fluid Mech.*, **224**, 77, 1991.
- [2] X.-Y. Lu and J. Sato. A numerical study of flow past a rotationally oscillating circular cylinder. *J. Fluids Struct.*, **10**, 829, 1996.
- [3] M.-H. Chou. Synchronization of vortex shedding from a cylinder under rotary oscillation. *Comput. Fluids*, **26**, 755, 1997.
- [4] S. Choi, K. Choi and S. Kang. Characteristics of flow over a rotationally oscillating cylinder at low Reynolds number. *Phys. of Fluids*, **14**(8), 2767, 2002.
- [5] Hartlen, R. T. and Currie, I. G. Lift-Oscillator Model of Vortex-Induced Vibrations. *Journal of Engineering Mechanics*, **96**(5), 577, 1970.
- [6] A. H. Nayfeh, F. Owis and M.R. Hajj. A model for the coupled lift and drag on a circular

cylinder. *Proc. of DETC 2003, ASME 19th Biennial Conference on Mechanical Vibrations and Noise*, Chicago, IL, USA, DETC2003/VIB-48455. 2003.

[7] Isam Janajreh and Muhammad Hajj. An Analytical Model for the Lift on a Rotationally Oscillating Cylinder. BBA VI International Colloquium on: Bluff Bodies Aerodynamics & Applications, Milano, Italy, July, 20–24 2008

[8] Y.C. Kim and E. J. Powers. Digital bispectral analysis and its applications to nonlinear wave interactions. *IEEE Trans. Plasma Sci.*, **PS-7** 120-131, 1979.

[9] M. R. Hajj, R. W. Miksad and E. J. Powers. Fundamental-subharmonic interaction: effect of the phase relation. *Journal of Fluid Mechanics*, **256**, 403, 1993.

[10] M. R. Hajj, R. W. Miksad and E. J. Powers. Perspective: measurements and analysis of nonlinear wave interactions with higher-order spectral moments. *Journal of Fluids Engineering*, 119 3, 1997.

[11] E. J. Powers and S. Im. Introduction to higher-order statistical signal processing and its applications. in: *Higher-Order Statistical Signal Processing* (Boashash, Powers & Zoubir eds.) Longman, Australia. 1995.

[12] A. H. Nayfeh *Perturbation Methods*, Wiley, New York. 1973.

[13] A. H. Nayfeh *Introduction to Perturbation Techniques*, Wiley, New York. 1981.